

## PREPARATION OF POROUS NANOCOMPOSITE SCAFFOLDS WITH HONEYCOMB MONOLITH STRUCTURE BY ONE PHASE SOLUTION FREEZE-DRYING METHOD\*

Yang Xu<sup>a,b</sup>, Duo Zhang<sup>b\*\*</sup>, Zong-liang Wang<sup>a</sup>, Zhan-tuan Gao<sup>a</sup>,  
Pei-biao Zhang<sup>a\*\*</sup> and Xue-si Chen<sup>a</sup>

<sup>a</sup> Key Laboratory of Polymer Ecobiomaterials, Changchun Institute of Applied Chemistry,  
Chinese Academy of Sciences, Changchun 130022, China

<sup>b</sup> Department of Plastic and Cosmetic Surgery, First Hospital of Jilin University, Changchun 130021, China

**Abstract** Biodegradable porous nanocomposite scaffolds of poly(lactide-co-glycolide) (PLGA) and L-lactic acid (LAc) oligomer surface-grafted hydroxyapatite nanoparticles (op-HA) with a honeycomb monolith structure were fabricated with the single-phase solution freeze-drying method. The effects of different freezing temperatures on the properties of the scaffolds, such as microstructures, compressive strength, cell penetration and cell proliferation were studied. The highly porous and well interconnected scaffolds with a tunable pore structure were obtained. The effect of different freezing temperature (4°C, -20°C, -80°C and -196°C) was investigated in relation to the scaffold morphology, the porosity varied from 91.2% to 83.0% and the average pore diameter varied from (167.2 ± 62.6) μm to (11.9 ± 4.2) μm while the  $\sigma_{10}$  increased significantly. The cell proliferation were decreased and associated with the above-mentioned properties. Uniform distribution of op-HA particles and homogeneous roughness of pore wall surfaces were found in the 4°C frozen scaffold. The 4°C frozen scaffold exhibited better cell penetration and increased cell proliferation because of its larger pore size, higher porosity and interconnection. The microstructures described here provide a new approach for the design and fabrication of op-HA/PLGA based scaffold materials with potentially broad applicability for replacement of bone defects.

**Keywords:** Freeze-drying; Scaffold; Hydroxyapatite; Nanocomposite; Honeycomb monolith structure.

### INTRODUCTION

Bone tissue engineering aims at the repairing and restoring damaged or diseased tissue function employing three fundamental “tools”, namely biological scaffolds, cells, and bioactive molecules<sup>[1]</sup>. Scaffolds are central components of tissue engineering because they provide a three-dimensional structure for *in vitro* or *in vivo* cells ingrowth and inducing tissue and organ regeneration<sup>[2]</sup>. They usually act as a temporary substitute for the extracellular matrix and must have both appropriate structural and functional properties<sup>[3, 4]</sup>.

Regarding the microstructures of 3-D scaffolds, highly porous (> 90%) and interconnected pore networks are desirable<sup>[5]</sup>. The higher porosity of scaffold provides more structural space for cell accommodation. Some evidence also showed that pore interconnectivity is as important as porosity for bone ingrowth, particularly in

\* This work was financially supported by the National Natural Science Foundation of China (Nos. 30772209, 50973109 and key project 50733003), the “863” (No. 2007AA03Z320) from the Ministry of Science and Technology of China, and Major Project of International cooperation from the Ministry of Science and Technology of China (No. 20071314).

\*\* Corresponding authors: Pei-biao Zhang (章培标), E-mail: zhangpb@ciac.jl.cn

Duo Zhang (张舵), E-mail: zhangduo2002@yahoo.com.cn

Received March 18, 2010; Revised April 7, 2010; Accepted April 22, 2010

doi: 10.1007/s10118-010-1015-5

the early stages of bone regeneration and penetration in the scaffold<sup>[6]</sup>. It's mainly because the interconnections in a porous biomaterial are the pathways for conducting cells, vessels, and nutrients or metabolites between the pores. Moreover, scaffold pore size has also been shown to influence cellular activity and tissue regeneration<sup>[7]</sup>. The optimal scaffold pore size varied with different cell types to allow maximal entry of cells as well as cell adhesion and matrix deposition<sup>[8]</sup>. It has been suggested that pore size of 5–15  $\mu\text{m}$  is suitable for fibroblasts, 20–125  $\mu\text{m}$  for adult mammalian skin tissues and 100–350  $\mu\text{m}$  for bone tissues. Therefore, a lot of researches have focused on successful cell infiltration and host tissue ingrowth developing methods for preparing scaffolds with suitable microstructures<sup>[9, 10]</sup>.

A widely used method to create pores is the thermally induced phase separation (TIPS) or namely freeze-drying. It is beneficial for those natural or synthetic polymers dissolved in water or organic media. When the temperature is low enough to allow the freeze of the solution, the phase separation mechanism would be solid-liquid demixing, which forms frozen solvent and concentrated polymer phases. The frozen solvent can be easily removed from the polymeric network by thawing, which may create voids and lead to a porous structure<sup>[11]</sup>. The porosity and pore size could be adjusted by varying the solution concentration, the freezing temperature and the freezing rate.

The previous works of our group focused on a novel composite of poly(lactide-*co*-glycolide) (PLGA) and hydroxyapatite (HA) nanoparticles surface grafted with poly(L-lactide) (PLLA) or L-lactic acid (LAc) oligomer, which was fabricated into three-dimensional (3D) scaffolds by a solvent-casting(or melt-molding)/particulate-leaching method for bone tissue engineering<sup>[12, 13]</sup>. However, the composite scaffolds fabricated with particulate-leaching method had two drawbacks, including the limited pore interconnection influencing the cell or tissue ingrowth, and the water immersion process blocking the growth factors or bioactive nutrients incorporated into scaffolds.

In the present study, the freeze-drying technique with 1,4-dioxane as a solvent was explored to fabricate porous nanocomposite scaffolds of PLGA and HA nanoparticles surface grafted with LAc oligomer (op-HA). The scaffolds with pore arrangement and highly interconnected macro/microporous structure were prepared with different freezing dry conditions. The pore microstructure, the surface topography and the mechanical properties, as well as the cell penetration and cell viability of these scaffolds were investigated, and the optimal production condition was assessed.

## MATERIALS AND METHODS

### *Materials*

L-lactide (LA) and glycolide (GA) were purchased from Purac, Holland. Cell culture grade chemicals were used including Dulbecco's modified eagle medium (DMEM, Gibco, USA), 3-{4,5-dimethylthiazol-2yl}-2,5-diphenyl-2H-tetrazoliumbromide (MTT, Sigma, USA), fetal bovine serum, trypsin-EDTA, penicillin and streptomycin (Gibco, USA), a tissue culture grade polystyrene plastic flasks and plates (Costar, USA). Newborn rabbit was purchased from the Institute of Experimental Animals of Jilin University, in accordance with the institutional guidelines for care and use of laboratory animals. Other reagents and solvents were of analytical grade and used as received.

### *Preparation of Porous Scaffolds*

Poly(lactide-*co*-glycolide) (PLGA, LA:GA = 8:2,  $M_w = 1.0 \times 10^5$ ) was synthesized in our laboratory. The synthesis of HA nanocrystals and their surface grafting with LAc oligomer have been reported in our previous works<sup>[13, 14]</sup>. The op-HA was needle-like nanoparticles of 100–300 nm in length and 30–40 nm in width. The amount of grafted LAc oligomer in op-HA used in this study was about 1.1 wt% analyzed with the method of weight loss using a thermogravimetry analysis (TGA) instrument (TA Instruments TGA500, USA).

The porous op-HA/PLGA composite scaffolds were fabricated with a modified freeze-drying method according to the references<sup>[11, 15]</sup>. First, PLGA was dissolved into dehydrated 1,4-dioxane at 20°C under magnetic stirring overnight. op-HA nanoparticles were dispersed in dehydrated 1,4-dioxane by ultrasonic treatment for 30 min and then mixed into the PLGA solution to prepare op-HA/PLGA composites. The

concentration of op-HA/PLGA in solution was 100 g/L. The content of op-HA in op-HA/PLGA was 20 wt%. Secondly, the solution was transferred into a polypropylene (PP) test tube with a thickness of 1 mm, 80 mm in length and 15 mm in diameter. The tubes were then frozen without any protection in order to permit solvent crystals growing from the tube walls toward the longitudinal axes of the tubes. To investigate the effects of different freezing temperatures on the porous structure, the samples were immediately quenched to 4°C, -20°C, -80°C (freezer) and -196°C (liquid nitrogen) for 24 h. Lastly, the frozen tubes were placed in a freezer and 1,4-dioxane was removed using vacuum drying at -4°C. The samples were then kept in a desiccator cabinet at room temperature.

#### **Environmental Scanning Electron Microscopy (ESEM) Observation**

An environmental scanning electron microscope (Model XL 30 ESEM FEG, Philips) was used to observe the morphology of the fracture surfaces of the obtained samples. The diameter of nearly 200 pores of each material was analyzed. The surface chemical composition of the specimens was examined using an energy dispersive X-ray analyzer (EDXA, Genesis2000). For ESEM observation, the samples were frozen in liquidized N<sub>2</sub>, and quickly broken off to obtain the random brittle-fractured surface. A layer of gold was sprayed uniformly over the fractured surfaces before the observation.

#### **Porosity Analysis**

The porosity of the composite scaffolds was determined using a modified liquid displacement method<sup>[16]</sup>. Briefly, a sample of initial weight  $W_i$  was immersed in a graduated cylinder containing 4 mL ethanol and kept for 24 h to allow the ethanol to penetrate into the pores of the scaffold completely. The total volume of the remaining ethanol and the ethanol-impregnated scaffold was then recorded as  $V_1$  by simply reading the level in graduated cylinder. The ethanol-impregnated scaffold sample was then removed from the graduated cylinder and immediately weighed as  $W_f$ . The residual ethanol volume in cylinder was recorded as  $V_2$  and the total volume of the scaffold was  $(V_1 - V_2)$ . The pore volume of the scaffold can be calculated from the volume of ethanol (density  $\rho_{\text{ethanol}} = 0.789 \text{ g}\cdot\text{cm}^{-3}$ ) resided in scaffold  $(W_f - W_i)/\rho_{\text{ethanol}}$ . Thus, the opening porosity can be determined using the following equation:

$$\text{Porosity} = [(W_f - W_i)/\rho_{\text{ethanol}}]/(V_1 - V_2)$$

#### **Compressive Strength Tests**

A universal testing machine (Instron 1121, UK) was employed to evaluate the compressive mechanical properties of the composite scaffolds. Cylindrical specimens with 10 mm in diameter and 10 mm in length were prepared and measured at a crosshead speed of 2 mm·min<sup>-1</sup>. The stress at 10% strain was recorded as  $\sigma_{10}$ . Three replicates were tested for each condition.

#### **Cell Viability Assays**

Osteoblasts were isolated and cultured according to our previous method<sup>[13]</sup>. The cell viability of osteoblasts on materials was determined using the MTT assay. The disks of porous scaffolds (11 mm in diameter, 5 mm in length) were prepared, repeatedly washed with deionized distilled water, and were sterilized by immersing into 70% ethanol for 30 min. The ethanol was then removed by soaking for 1 h in 3 changes of 0.1 mol/L PBS. The scaffolds were placed in 24-well tissue culture plates and pre-wetted by immersing in the culture medium at 4°C for 24 h. The obtained osteoblasts were seeded onto the top of the scaffolds ( $2.0 \times 10^6$  cells/100  $\mu\text{L}$ /scaffold) and left undisturbed in an incubator for 4 h to allow the cells to attach to them. Then each well was supplemented with an additional 1 mL of culture medium. The plates were returned to a humidified incubator and cultured at 37°C with 95% air and 5% CO<sub>2</sub> for 1, 3 and 7 days. The medium was refreshed every two days. Four hours before each culture interval, 80  $\mu\text{L}$  of MTT (5 mg·mL<sup>-1</sup> in PBS) was added to each well and the cells were incubated for an additional 4 h. The medium was removed and 800  $\mu\text{L}$  of acidified isopropanol (0.2 mL of 0.04 mol/L HCl in 10 mL of isopropanol) was added to each well to solubilize the converted dye. The solution in each well was mixed completely and 150  $\mu\text{L}$  of the solution of each well was transferred to another 96-well plate (Costar), and optical density was measured at 540 nm wavelength on a Thermo Electron MK3

spectrophotometer. The mean value of the three readings for each sample was used as the final result.

#### **Observation of Cell Penetration and Attachment**

Cell penetration and attachment were analyzed with microscopical observation (ESEM). The osteoblasts were seeded onto the porous scaffolds according to the above mentioned method, and cultured for 3 days *in vitro*. The samples were rinsed with PBS three times and fixed with a 3% glutaraldehyde solution for 1 h. In the following steps, the samples were processed by soaking them in an osmium tetroxide solution for 1 h, and then dehydrated through a series of ethanol solutions with graded concentrations followed by two changes of 100% amyl acetate for 15 min each. The samples were then freeze-dried and their transects were observed with ESEM.

#### **Statistics**

The data were expressed as mean  $\pm$  standard deviation. Statistical analysis was performed with Origin 7.0 (OriginLab Corporation, USA). One-way analysis of variance (ANOVA) was used to compare two different groups. A *p* value of  $< 0.05$  was considered to be statistically significant.

### **RESULTS AND DISCUSSION**

It was well known that TIPS is one of the most important and popular techniques for producing 3D porous scaffolds with natural or synthetic polymers that are widely used in tissue engineering. With TIPS processes, scaffolds with high porosity can be manufactured. With the first method of TIPS, the scaffolds were obtained with large porosities (up to 95%) but small pore sizes (13–35  $\mu\text{m}$ )<sup>[17]</sup>. The factors that can affect the formation of the solvent crystals such as type of the solvent and polymer, concentration of the polymer solution and speed of the crystallization would affect morphology structure of the obtained scaffold<sup>[18]</sup>.

This study aimed to develop a porous nanocomposite scaffold of op-HA/PLGA with honeycomb monolith structure using 1,4-dioxane as a solvent. Compared with those produced with the particulate leaching method in our previous work<sup>[12, 13]</sup>, some prospective properties, including high porosity, high interconnection, direct molding at a lower temperature and processing without water leaching were reached with this method.

#### **Microstructures**

SEM micrographs show that the pores of all scaffolds were tubal and interconnected (Fig. 1). Obviously, the tubal pores were arranged in solvent crystal growing directions (see Scheme 1).

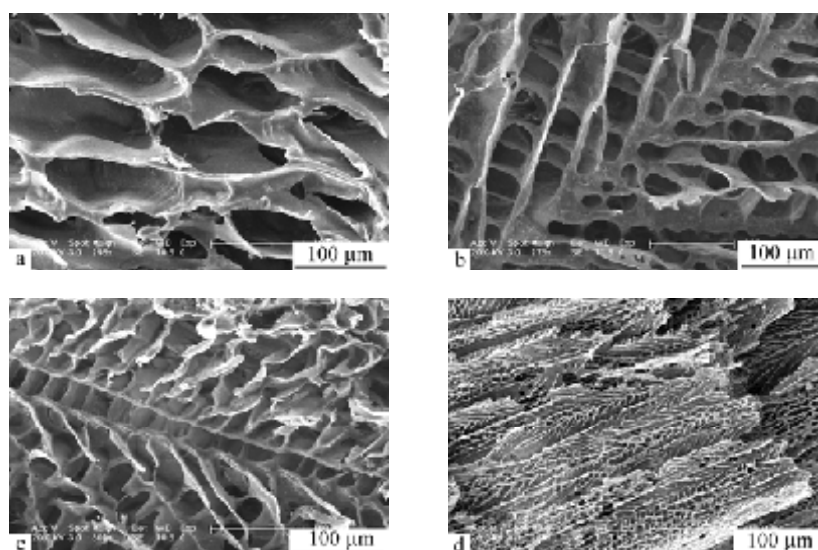
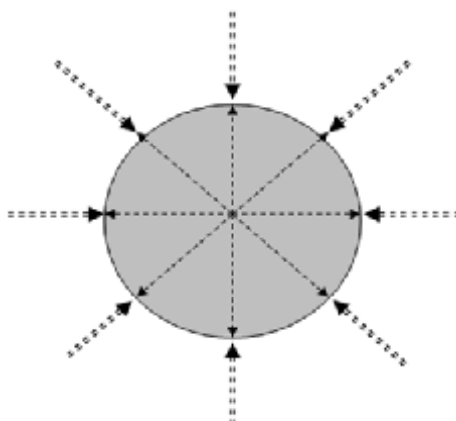


**Fig. 1** SEM micrographs of transverse sections of the nanocomposite scaffolds of op-HA/PLGA with a honeycomb monolith structure fabricated with freezing temperatures of 4°C (a), -20°C (b), -80°C (c) and -196°C (d)



**Scheme 1** Relationship between porous structures and pore growing directions in the one phase solution freeze-drying method

The double line arrows indicate the direction of freezing (or pore growing direction) and the single line arrows indicate the pore alignment in a cylindrical scaffold.

More recently, 1,4-dioxane, which has a melting point of approximately 11°C, has been used successfully as a freezing vehicle, allowing more flexibility in the process as it can be frozen and easily sublimed at 4°C temperature<sup>[19]</sup>. Using 1,4-dioxane as a solvent, the temperature gradient-guided TIPS, in which the temperature gradient existed during the phase separation, could produce the microtubules-like porous-structured scaffolds<sup>[15]</sup>.

In this study, directional solvent crystals were formed in a tubal device during freezing of the op-HA/PLGA/1,4-dioxane solution at different temperature regimes without a specially devised method. A homogeneous insulation cover allows cooling from the sides, bottom and top simultaneously at a lower cooling rate, such as at 4°C freezing temperature; however, when freeze-casting is performed within the range from -20°C to -196°C, the heat-transfer gradient and the direction of freezing are mostly from the sides to the centre of tubes (diameter approx. 11 mm) because of their rapid cooling rates. A greater alignment of the pores was observed at lower freezing temperatures due to the larger driving force of the 1,4-dioxane dendrites during the solidification process as a direct consequence of the greater heat transfer gradient<sup>[9]</sup>.

#### **Pore Size and Porosity**

As shown in Fig. 1, the significant differences in pore size were observed with SEM analysis. The SEM micrographs show that the largest pore size was in the group of 4°C among these four groups (Fig. 1a). In the groups of -20°C, -80°C and -196°C (Figs. 1b–1d), though the shapes of the macroporous structures were quite similar, their macropore sizes in the bulk samples were different from each other. It indicated that the pore size was associated tightly with the freezing temperatures.

The above-mentioned results were further proved by analysis of pore diameter. Figure 2 shows the frequency distribution of pore diameters of op-HA/PLGA scaffolds based on different freezing temperatures. The results suggested that the average pore sizes of 4°C, -20°C, -80°C and -196°C were  $(167.2 \pm 62.6) \mu\text{m}$ ,  $(52.6 \pm 20.4) \mu\text{m}$ ,  $(28.0 \pm 8.9) \mu\text{m}$  and  $(11.9 \pm 4.2) \mu\text{m}$  respectively. Obviously, small diameter foam bubbles were produced more easily at low freezing temperatures. When a relatively higher freezing temperature was adopted, larger average pore size and a wider pore size distribution were obtained. It is confirmed that the cooling rate (the solvent crystal growth rate) clearly affects the solvent crystal size (in turn the pore sizes).

The effect of different freezing temperatures on the porosity of the op-HA/PLGA scaffolds is shown in Table 1. As expected, at the level of a 100 g/L composite solution, the porosities of the scaffolds decreased linearly from  $(91.2 \pm 0.8)\%$  to  $(83.0 \pm 0.6)\%$  while the freezing temperature was decreased from 4°C to -196°C. It was indicated that the nucleation temperature during a freezing process not only had a great effect on the pore alignment and pore size distribution, but also had an effect on the overall level of porosity.

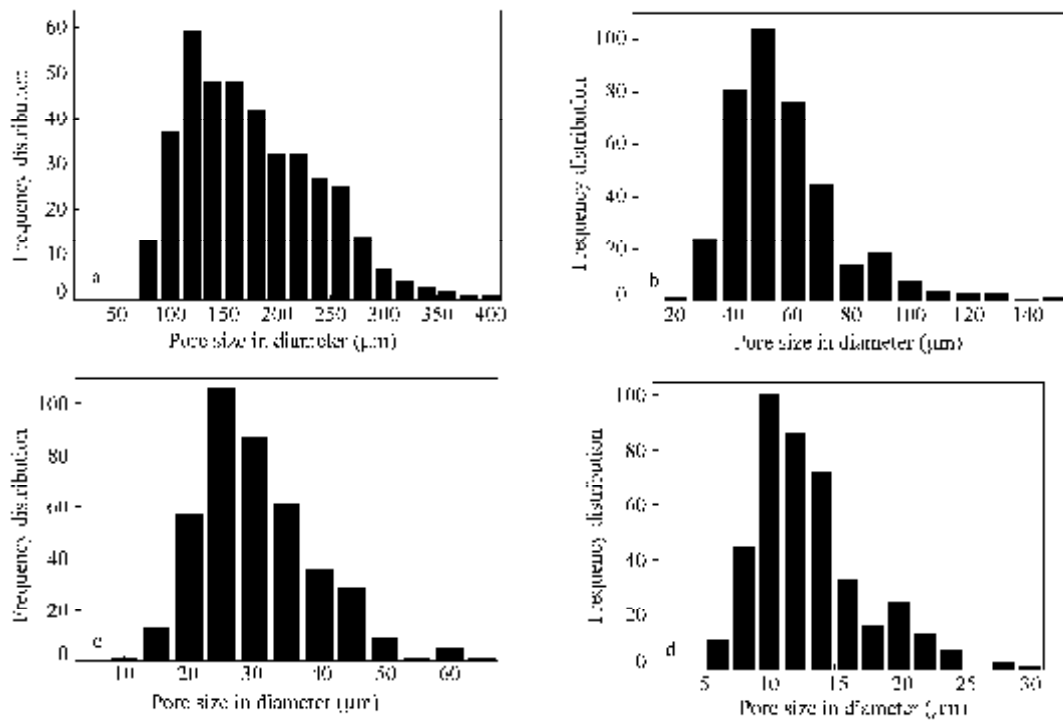


**Fig. 2** Frequency distribution of pore diameters of op-HA/PLGA scaffolds based on different freezing temperatures: 4°C (a), -20°C (b), -80°C (c) and -196°C (d)

**Table 1.** Porosity and compressive mechanical parameters of the op-HA/PLGA scaffolds fabricated with freezing-dry method

Freezing temperature (°C)	Porosity (%)	$\sigma_{10}$ (MPa)
4	91.2 ± 0.8 <sup>a</sup>	0.52 ± 0.09
-20	87.7 ± 2.4 <sup>b</sup>	0.63 ± 0.05
-80	85.9 ± 1.8	0.68 ± 0.06
-196	83.0 ± 0.6	0.98 ± 0.14 <sup>*</sup>

<sup>\*</sup>  $p < 0.05$  compared with the other groups;

<sup>a</sup> and <sup>b</sup>  $p < 0.05$  compared with -80°C or -196°C, respectively

### Surface Properties of Pore Walls

Surface topography and surface element composition of pore walls were analyzed with ESEM and EDX (Fig. 3). It is reported that surface properties, both chemical and topographical properties, can control and affect cellular adhesion, proliferation and differentiation<sup>[20]</sup>. As shown in Figs. 3(a)–3(d), rough surfaces of the pore walls were observed in all groups. Nano-sized op-HA particles were uniformly distributed on the surface of pore walls and few large aggregates were observed. The crystals were embedded in the walls and presented on the surfaces. The group of 4°C (Fig. 3a) exhibited more homogeneous roughness of the wall surface in a pore compared with the others (Figs. 3b–3d). The reason is deduced that the higher freezing temperature would lead to formation of larger solvent crystals formation. As the freezing temperature decreased from -20°C to -196°C, the surface topography became more irregular and the nanoparticles on the wall surface heaved more obviously (Figs. 3b–3d).

EDX analysis showed that plenty of calcium (Ca) and phosphor (P) elements existed on the pore walls of all the groups (Fig. 3e). The levels of Ca and P exposure on the surfaces of -20°C and -80°C scaffolds (Fig. 3e-2 and 3e-3) were obviously higher than those of the others (Fig. 3e-1 and 3e-4). More op-HA nanoparticles exposed on the pore walls contributed to the higher contents of Ca and P in op-HA/PLGA nanocomposite scaffolds. The lower contents of Ca and P in the -196°C scaffold (Fig. 3e-4) might result from

distribution of most HA nanoparticles in deep ravines (Fig. 3d) which could not be detected by the energy dispersive X-ray analyzer. Therefore, the results indicated that the freezing temperature could affect the distribution of op-HA particles and the contents of Ca and P on the pore wall surface of scaffold to some extent.

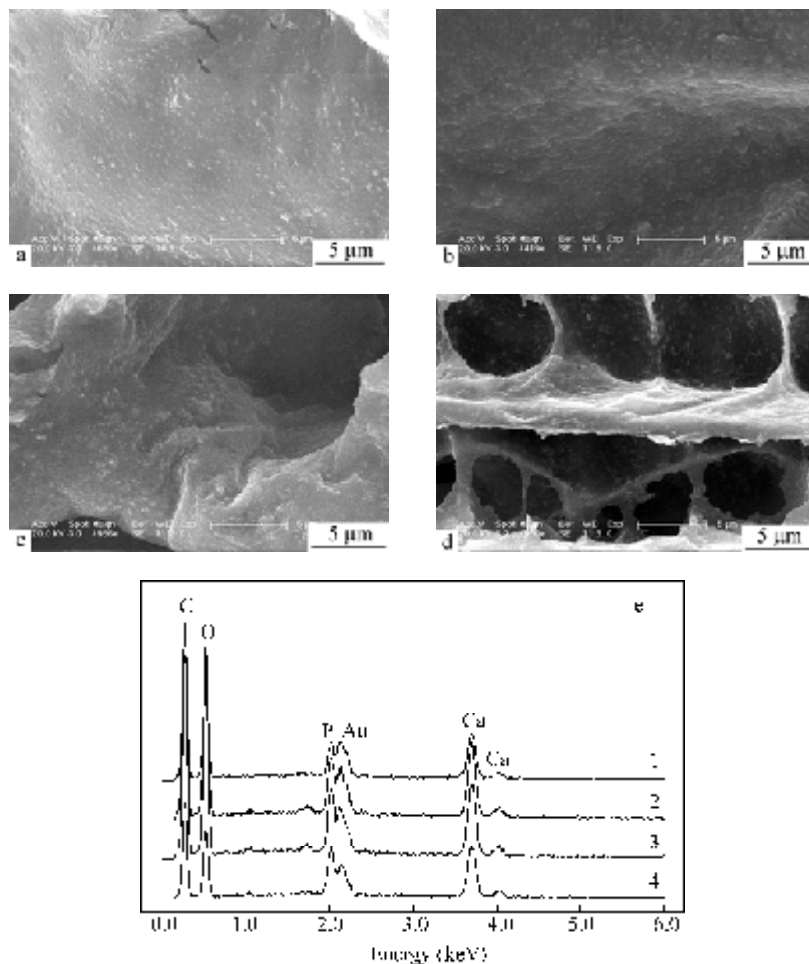


**Fig. 3** Pore wall surface topography (a–d) and EDX curves (e) of the porous scaffolds fabricated with the freeze-dry method by different freezing temperatures: 4°C (a and e-1), –20°C (b and e-2), –80°C (c and e-3) and –196°C (d and e-4)

It is well known that the nano-scale HA particles have the smallest average grain size of less than 100 nm, which could provide the greatest specific surface area. Nanophase materials possess increased grain boundaries at the surface (due to the smaller grain size), which benefits cell adhesion and proliferation. It has been reported that osteoblast adhesion appears primarily at the grain boundaries<sup>[21]</sup>. The freeze-drying method in this study afforded more regular arrangement of pores and rougher surfaces formed on the pore walls because of a higher degree of exposure of op-HA particles on the material surface in freeze-drying scaffolds.

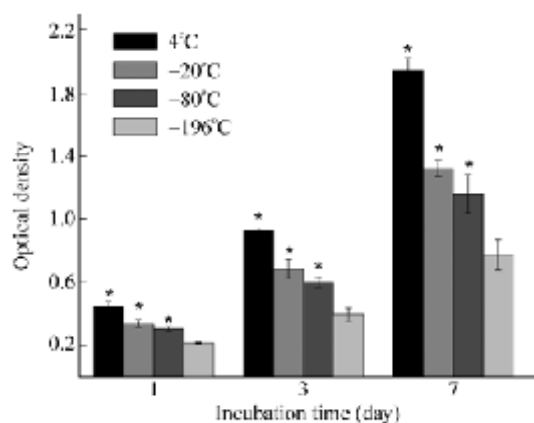
### **Compressive Strengths**

Table 1 also shows the effects of the freezing temperature on the compressive mechanical properties of the porous op-HA/PLGA scaffolds. The  $\sigma_{10}$  increased from 0.52 MPa to 0.98 MPa with decreasing freezing temperature from 4°C to –196°C. As the freezing temperature was decreased from 4°C to –196°C, there was nearly a one-fold increase in the  $\sigma_{10}$ . However, the  $\sigma_{10}$  values changed slightly as the freezing temperature was decreased from 4°C to –80°C. The differences in pore arrangement, porosity and pore size are some of the main

factors that may have contributed to the variations in the mechanical properties of the scaffolds. It should be noted that the compressive strengths obtained in this study are comparable or even much higher than those reported in the literature<sup>[9, 16, 17, 22]</sup>, because of the construction of the aligned pores and the formation of strong walls containing op-HA nanoparticles.

### Cell Viability

Osteoblasts are cell type for assessment of orthopaedic biomaterials. Figure 4 shows the OD values of rabbit osteoblasts growing on different samples after 1, 3 and 7 days *in vitro* culture. It was an initial stage for osteoblasts attaching and growing on the scaffolds in 1 day to 3 days after cell seeding. The results of 3 days' culture show that there were significant differences in cell numbers among the scaffolds fabricated at different freezing temperatures ( $p < 0.05$ ). There was the highest cell numbers in the group of 4°C freezing temperature. The attached cell number decreased significantly as the freezing temperature of the scaffolds varying from 4°C to -196°C. The similar differences among these groups were kept from 3 days' to 7 days' culture. From 3 days' to 7 days' culture, a nearly 2-fold increase in cell number of each group was observed. The results of cell culture indicate that the scaffolds fabricated with higher freezing temperature could provide more 3D spaces for cell ingrowth because the higher porosity, larger pore diameter and a higher degree of interconnection.



**Fig. 4** OD values of osteoblasts growing on the different composite scaffolds at various incubation periods  
\* $p < 0.05$  compared with the other groups

### Cell Penetration and Adhesion

ESEM analysis were carried out for further investigation on cell penetration and cell adhesion after the osteoblasts were seeded on the scaffolds and cultured for 3 days (Figs. 5 and 6). All the scaffolds exhibited good biocompatibility that the osteoblasts were attached and spread well on the surfaces of the materials. Homogeneously rough surfaces are beneficial for cell adhesion and spreading<sup>[23]</sup>. The initial cell adhesion and spreading are known to affect the long-term phenotype of anchorage-dependent cells. In the nanoscale, osteoblast adhesion is independent of the ceramic surface chemistry and material phase, but depends on the topography of the nanophase ceramics<sup>[24]</sup>. In the group of 4°C freezing temperature, the attached cells were observed simultaneously in the top, centre and bottom areas of the scaffolds where the cell density along the depth direction was homogeneous and a maximum cell penetration depth was about 5 mm (Fig. 5). However, a small amount of osteoblasts could be found in the other scaffolds and the cell densities along the depth direction were not homogeneous. The cells were most abundant on the surface and the cell density gradually decreased with depth increasing (Fig. 6). Especially, the cells could only be observed on the surface of the scaffold of -196°C freezing temperature (Fig. 6c). This result indicates that the significant cell penetration depth was because of the large and highly interconnected pores of a scaffold.

In a word, scaffold should be designed so as to improve cell and nutrient transfer to the scaffold center, and

provide enough space and suitable surface properties for supporting cell adhesion, spreading and growth<sup>[2]</sup>. Besides the freezing temperature, solution concentration is another critical factor to control the porosity and microstructure of a scaffold in TIPS. Therefore, in the future studies, the effects of solution concentration or both solution concentration and freezing temperature on the formation of highly porous structures of the op-HA/PLGA nanocomposite will be further investigated.

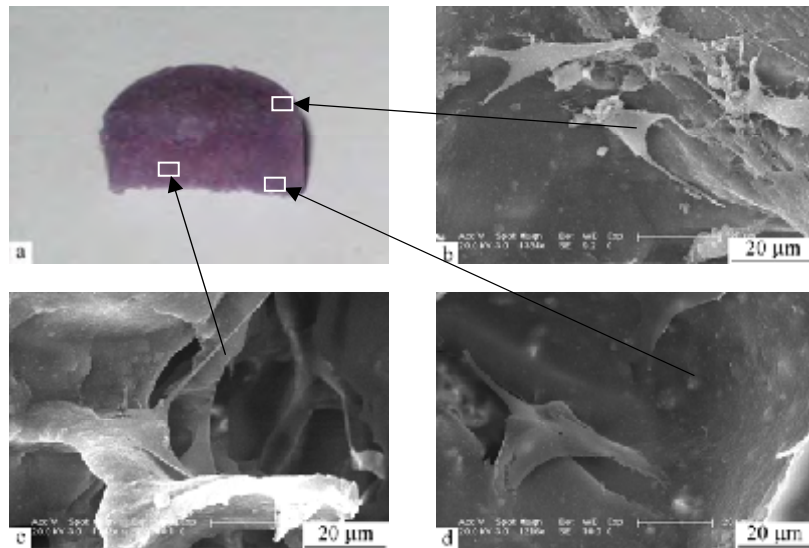


**Fig. 5** ESEM micrographs of vertical sections of the composite scaffold fabricated with 4°C freezing temperature after incubating osteoblasts for 3 days  
a) Macroscopic observation; b)–d) Micrographs at the top (b), centre (c) and bottom (d) areas (indicated by arrows) of the sample, respectively

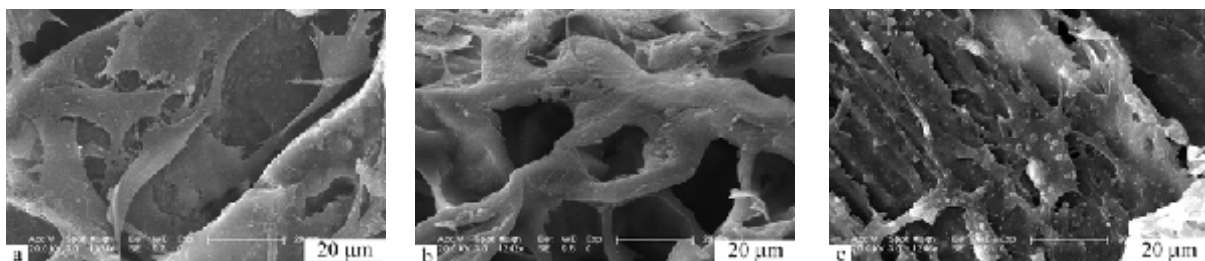


**Fig. 6** ESEM micrographs of the different porous scaffolds seeded with osteoblasts and incubated for 3 days with freezing temperature of  $-20^{\circ}\text{C}$  (a),  $-80^{\circ}\text{C}$  (b) and  $-196^{\circ}\text{C}$  (c), respectively  
The interior areas of vertical sections (a, b) or the surface areas (c) were observed.

## CONCLUSIONS

Porous nanocomposite scaffolds of op-HA/PLGA with a honeycomb monolith structure were prepared by the one phase solution freeze-drying method in this study. The freezing temperature played a critical role in formation of the highly porous structure with a high degree of interconnection. The average pore diameter varied from  $(167.2 \pm 62.6) \mu\text{m}$  to  $(11.9 \pm 4.2) \mu\text{m}$  as the freezing temperatures were changed from  $4^{\circ}\text{C}$  to  $-196^{\circ}\text{C}$ . The  $4^{\circ}\text{C}$  freezing temperature scaffold showed better cell penetration and increased cell proliferation because of its larger pore size, higher porosity and interconnection. Although its compressive mechanical property was lower than that of the others, it will be acceptable for replacement of nonbearing bone. The further study will focus on the preparation of scaffolds with both highly porous structures and high mechanical properties by adjusting the production conditions including solution concentration, freezing temperature and freezing rate.

**REFERENCES**

- 1 Biondi, M., Ungaro, F., Quaglia, F. and Netti, P.A., *Adv. Drug. Deliv. Rev.*, 2008, 60: 229
- 2 Chen, P., Ushida, T. and Tateishi, T., *Macromol. Biosci.*, 2002, 2: 67
- 3 Badylak, S.F., *Cell Dev. Biol.*, 2002, 13: 377
- 4 Li, M.Y., Bidez, P., Guterman-Tretter, E., Guo, Y., MacDiarmid, A.G., Lelkes, P.I., Yuan, X.B., Yuan, X.Y., Sheng, J., Li, H., Song, C.X. and Wei, Y., *Chinese J. Polym. Sci.*, 2007, 25: 331
- 5 Hamasaki, S., Tachibana, A., Tada, D., Yamauchi, K. and Tanabe, T., *Mater. Sci. Eng. C*, 2008, 28: 1250
- 6 Gutierrez, M., Lopes, M.A., Hussain Sooraj, N., Lemos, A.F., Ferreira, J.M.F., Afonso, A., Cabral, A.T., Almeida, L., and Santos, J.D., *Acta Biomater.*, 2008, 4: 370
- 7 O'Brien, F.J., Harley, B.A., Yannas, I.V. and Gibson, L., *Biomaterials*, 2004, 25: 1077
- 8 Sosnowski, S., Woźniak, P. and Lewandowska-Szumiel, M., *Macromol. Biosci.*, 2006, 6: 425
- 9 Macchetta, A., Turner, I.G. and Bowen, C.R., *Acta Biomater.*, 2009, 5: 1319
- 10 Mikos, A.G., Johnna, S. and Temenoff, J.S., *EJB Electronic J. Biotech.*, 2000, 3: 1
- 11 Ho, M.H., Kuo, P.Y., Hsieh, H.J., Hsien, T.Y., Hou, L.T., Lai, J.Y. and Wang, D.M., *Biomaterials*, 2004, 25: 129
- 12 Zhang, P., Hong, Z., Yu, T., Chen, X. and Jing, X., *Biomaterials*, 2009, 30: 58
- 13 Cui, Y., Liu, Y., Cui, Y., Jing, X.B., Zhang, P.B. and Chen, X.S., *Acta Biomater.*, 2009, 5: 2680
- 14 Qiu, X.Y., Chen, L., Hu, J.L., Sun, J.R., Hong, Z.K., Liu, A.X., Chen, X.S. and Jing, X.B., *J. Polym. Sci. Part A: Polym. Chem.*, 2005, 43: 5177
- 15 Kim, J.W., Taki, K., Nagamine, S. and Ohshima, M., *Langmuir*, 2009, 25: 5304
- 16 Kothapalli, C.R., Shaw, M.T. and Wei, M., *Acta Biomater.*, 2005, 1: 653
- 17 Yang, F., Qu, X., Cui, W.J., Bei, J.Z., Yu, F.Y., Lu, S.B. and Wang, S.G., *Biomaterials*, 2006, 27: 4923
- 18 Nam, Y.S. and Park, T.G., *J. Biomed. Mater. Res.*, 1999, 47: 8
- 19 Schugens, C., Maquet, V., Grandfils, C., Jerome, R. and Teyssie, P., *J. Biomed. Mater. Res.*, 1996, 30: 449
- 20 Salgado, A.J., Coutinho, O.P. and Reis, R.L., *Macromol. Biosci.*, 2004, 4: 743
- 21 Webster, T.J. and Ejiogor, J.U., *Biomaterials*, 2004, 25: 4731
- 22 Thomson, R.C., Yaszemski, M.J., Powers, J.M. and Mikos, A.G., *Biomaterials*, 1998, 19: 1935
- 23 Gough, J.E., Notingher, I. and Hench, L.L., *J. Biomed. Mater. Res. A*, 2004, 68: 640
- 24 Li, B., Chen, X., Guo, B., Wang, X., Fan, H. and Zhang, X., *Acta Biomater.*, 2009, 5: 134